Space experiments using superconducting magnet technology

F N Werfel, U Floegel-Delor, T Riedel, P Schirrmeister, R Koenig, V Kantarbar, and O Vakaliuk

Adelwitz Technologiezentrum GmbH (ATZ), Naundorfer Str. 29, 04860 Torgau, Germany

Email: werfel@t-online.de

Abstract. We report on a fast-track experiment on the International Space Station (ISS) with the Earth's magnetic field, which has been recognized as a major task for a better understanding of our planet. For this purpose, YBCO bulk superconductors have been prepared, transported and stored on board the ISS. The properties of single grain superconducting bulk will be investigated before and after the ISS experiments. In parallel, the magnetic interaction between B_{Earth} and our YBCO bulk was investigated. An external 3D Helmholtz coil cancels unwanted electromagnetic fields down to 5 µT. Highly sensitive flux-gate sensors monitored the magnetic configuration as the ceramic plate was cooled to cryogenic temperatures. Shielding and field concentration effects of the Earth's magnetic field were observed and discussed. Thermally induced magnetic flux compression for future long-duration space missions was successfully tested, enabling future spacecraft shielding and braking functions.

1. Introduction

Since time immemorial, the space around our Earth has been a place of longing and scientific curiosity. We seek answers to questions such as: How did space evolve? Where do we come from? Do civilizations exist on other planets? The Earth's magnetic field in general is an important task for a better understanding of our planet and everywhere.

The magnetic field has reliably protected our planet for millions of years. The experiment presented here on Earth and in space was carried out in 2014-18 during the "Blue Dot" mission of German astronaut Alexander Gerst. The experiment investigated the interaction of the Earth's magnetic field with a superconductor. Initial results have been published [1, 2]

Space conditions open a wide range of possibilities for conducting conductive and inductive magnetic experiments and interactions under conditions of microgravity, low temperature, and low pressure. Each of these conditions has its unique advantages and disadvantages. For superconducting magnetic bearings (SMBs), well-known in the community since the discovery of high-temperature superconductors (HTS), the ideal environment is that of a deployed spacecraft in near zero gravity. On our Moon, gravity is less than 20% of that on Earth. In addition, the Moon has a combination of cold and vacuum. This favors the use of SMBs there to support rotary or linear magnetic devices designed for extreme functions, such as precisely moving a large load or maintaining fast rotation in a momentum flywheel. Both of these functions could be very useful for a future unmanned lunar observatory or a sun-tracking solar panel power system. Unlike on Earth, SMBs in microgravity have no counterbalancing forces. The conditions for setting up observatories there are favorably different from those on Earth. In a groundbreaking space-related SBIR-supported work [3], we have shown that magnetic levitation

can eliminate the conduction heat losses of a cryotransfer line by using non-contact magnetic levitation support. This novel transfer line offers the potential for significant cryogen savings, thus reducing the cost of cryogen use (experimental ~30% reduction). A smart passive 6 kg warm support with no control electronics, driven only by temperature variation, demonstrated the preferred applicability of the mechanical system, especially under space conditions.

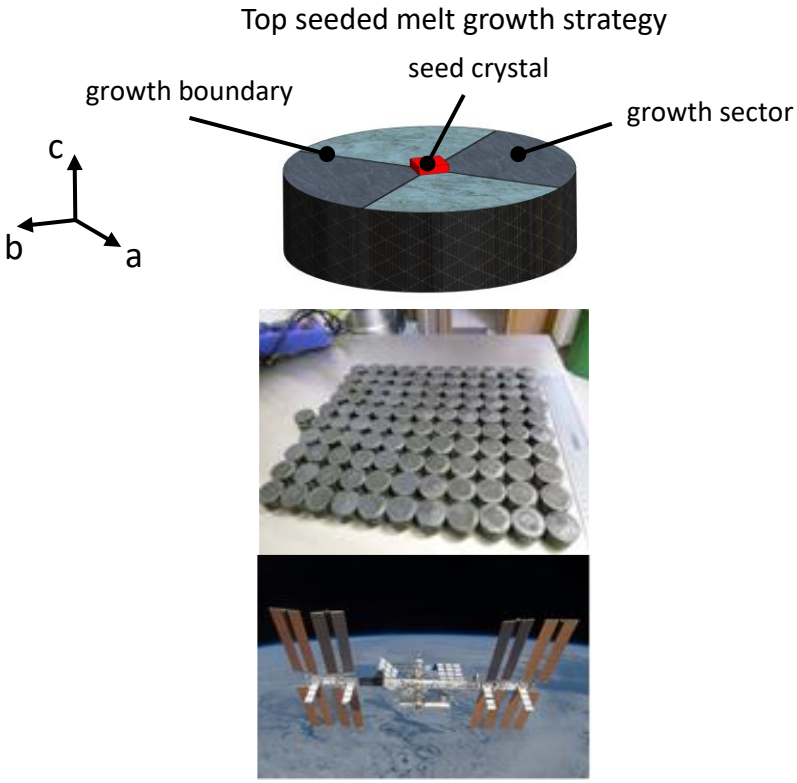

Figure 1. Superconductor experiments under space conditions; structure of melt textured REBCO bulk (top), production (center), and storage on ISS (bottom).

This report has a dual structure. We investigate and experimentally study the ability of YBCO bulk superconductors to influence weak magnetic fields for space applications. This study includes magnetic field generation, shielding, flux exclusion, and flux compression. The magnitude of the flux density is scaled to the level of the Earth's magnetic field B_{Earth} and varies between 30-60 μT, utilizing and indicating the Meissner effect phenomenon as the basis of the Type I superconductor state [4-7].

Highly sensitive flux-gate sensors are used to systematically measure the magnetic field generated around the conductor. We have studied the Earth magnetic field interaction of a 10 cm long and 0.8 kg superconductor in the non-superconductive state (warm) and in the superconducting state (cold). Both phases of the same material produce quite different shielding properties. We describe the physical laws of a perfectly conducting body versus a superconducting body. The physical consequences of interaction with an external magnetic field are shown. In contrast to active superconducting coils and magnets, which have been studied intensively in the last two decades, our investigations are limited to the easily exploitable Earth magnetic field by passive interaction [8-11].

From there, researchers can gain insight into how a fast-moving magnetic field affects the properties of the conductor body in space. The expected changes in the Earth's magnetic field structure of the YBCO conductor (Figure 1) are of particular interest for engineering applications such as

shielding and magnetic pressure performance. The results are valuable for further astrophysical discussions on why planets such as Venus and Mars exist without magnetic fields.

2. Magnetic interaction models

2.1. Perfect electric conductor

A perfect conductor, rather than a superconductor, would maintain an applied constant external magnetic field within its interior. This would not be dissipated even if the material had zero resistivity. We can show how this conclusion follows from Maxwell's equations for a perfect conductor. The field distribution in a perfect conductor (pc) obeys Faraday's law. A uniform external field B_0 in one direction means that the field inside the perfect conductor will be in the same direction. Its strength decreases exponentially with the thickness of the material. The field inside the perfect conductor shown in Figure 2 satisfies the exponential equation:

$$\frac{\partial B(z,t)}{\partial t} = \frac{\partial B_0(t)}{\partial t} e^{-z/\lambda} \qquad \lambda = \left[\frac{m}{\mu_0 n_{pc} q^2}\right]^{1/2} \quad \text{for a perfect conductor (pc),} \qquad (1)$$

where λ is the penetration depth at which the magnetic field becomes weaker by a factor of e, m is the mass of the charged carriers, their number n_{pc} and charge q, μ_0 is the permeability of free space. Any change in the external magnetic field B_0 is attenuated exponentially with the distance below the surface of the perfect conductor. If the value of λ is the depth of penetration, then the field will not change within the bulk of the perfect conductor. However, this does not mean that the magnetic field must be expelled from the interior. Magnetic flux expulsion requires B = 0, not $\partial B/\partial t = 0$. What is needed to make a magnet-superconductor interaction with B = 0?

2.2. Meissner Effect on Superconductors

Additional assumptions are needed to explain the Meissner effect in a superconductor [5]. The first criterion is the transition to a new electric and magnetic phase when a material is cooled below a critical temperature (T_c). The magnetic transition is much less obvious than its zero electrical resistance. When a magnetic field is applied to a superconducting sample, the field is excluded so that B = 0 throughout its interior.

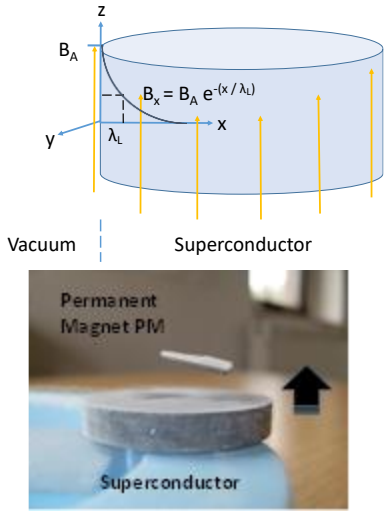

Figure 2. Perfect conductor and Meissner effect on bulk superconductor; Meissner surface currents J_s screen an external field B_A (top); PM gradually lifts-up.

This property of the superconducting state is known as the Meissner effect. It is a clear indication of a superconducting phase. Its mechanism shows that the external field is cancelled in the interior material by an opposing magnetic field generated by a steady shielding current flowing at the surface of the superconductor. As the YBCO material is cooled through the transition, the Meissner effect occurs in a highly dynamic process. The effect is achieved by rapidly decreasing the electrical resistivity, which dramatically increases the eddy current flux exclusion. This prevents the shielded region from trapping any flux. While the Maxwell equations cannot predict the Meissner property, the London and Maxwell equations together can lead to a prediction of the Meissner effect. At low field interaction in a superconductor, a constant current flows with $\partial J_s/\partial t = 0$ and the zero electric field $E = 0$. The normal current density is zero, all of the constant current density is carried by superconducting electrons e.

$$\nabla J_s = (1/\lambda_L{}^2)\, J_s \quad \text{with } \lambda_L = \left[\frac{m}{\mu_0 n_s e^2}\right]^{1/2} \qquad (2).$$

Equation 2 and Figure 2 show the transition from a perfect conductor (pc) to a superconductor (s) with the Meissner effect and λ_L the London penetration depths. The direction of the flowing surface currents in a superconductor is such that they generate a magnetic field that completely cancels the applied field. Such exclusion of magnetic fields in the Meissner state distinguishes a superconducting phase from a perfect conductor with the exponential penetration depth mentioned above.

The Earth's magnetic field is always present but is not considered in most HTS applications. In combination with μ-metal and low-T_c superconductors, very low static magnetic fields of 10^{-10} T could be obtained using the Meissner effect. Unfortunately, a perfect Meissner state in bulk HTS materials is extremely difficult to achieve in practice. Even textbooks and discussions in the literature mix and confuse Meissner and pinning effects, showing pictures of a PM several centimeters stably suspended above a cooled superconductor. In 99% of the cases, the levitation effect is pinning, not Meissner.

Now we compare the Earth's magnetic field with the YBCO HTS material. At 77 K the first critical magnetic field values of YBCO are B_{c1} (||) ~ 14 mT and B_{c1} (⊥) ~ 6 mT, a factor of 200 greater than the Earth's magnetic field B_{Earth} = 50 μT [7]. The otherwise very valuable pinning center structure in the Type-2 material, which is responsible for the ability to trap high magnetic fields for applications, prevents perfect shielding of very low and stray magnetic fields. In other words, it is the conductivity of our material that makes it so difficult to completely eliminate the trapped flux.

Coupled with the bulk space applicability of HTS, several steps in the development program convinced us to test flux shielding and compression in detail. First, we found in our experiments that no matter how carefully the HTS bulk tiles were grown and prepared, due to the strong pinning behavior, the low Earth magnetic field of about 48 μT was always trapped in our bulk material. A Helmholtz coil was installed around the experimental setup to partially or fully compensate for the Earth's magnetic field. In YBCO, however, the Earth's magnetic field generates the Meissner screening currents in a very thin surface layer of less than 1 μm. Maxwell's curl $B = \mu_0 J$ with B_{Earth} ~ 45 μT causes a small magnitude of the screening currents. For YBCO, a type II superconductor, the penetration depth of the earth field, according to F. London, is between 150 nm and 500 nm [6]. The depth λ_L also depends on the temperature.

3. B_{Earth} laboratory experiments

The Earth's magnetic field has been observed by satellites since the 1960s. The field shields the Earth's surface from the direct impact of the solar wind. The volume and geometry of the Earth's magnetic field is called the magnetosphere and has teardrop shape. It is round where it faces the sun's solar wind. Its tail is very long and waves like a flag in the solar wind. The strength of the Earth's magnetic field falls off as a dipole with $B = B_{Earth}\,(r_{Earth}/r)^3$ and is proportional to r^{-3}.

Laboratory measurements were made in a setup with FCL100 flux gate Hall sensors (Dr. Mayer, Germany). The earth's magnetic field is always present during our experiments. For our company site

in Torgau (85 m NN), Germany, the components of the Earth's magnetic field according to the NOAA National Geophysical Data Center are: horizontal 19 181 nT, vertical 45 363 nT, and total 49 251 nT.

3.1. Earth magnetic screening

First, a Helmholtz coil is used to compensate for the inevitable field trapping of B_{Earth} in YBCO plates. Another way to achieve field-free cooling is the geometric orientation of the YBCO plate parallel to the Earth's magnetic field vector. First, the Earth magnet field vector (B_{Earth} || a, b crystal) and the YBCO is cooled below T_c. Due to the crystal texture of the sample, the above small horizontal vector component of about 20 µT is trapped during the field cooling (fc) process. In the following experiment, shown in Figure 3, the fluxgate sensor measures the magnetic field behind the shielded YBCO plate. B_{Earth} is extensively shielded and follows an exponential decay perfectly (Figure 3). Small deviations in the shielding behavior between the experiment and model are still observed when measuring directly on the back surface, which shows a residual trapped field depending on the size of the YBCO plate.

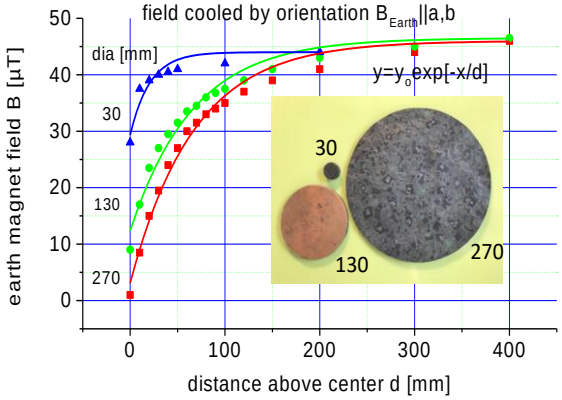

Figure 3. Measured Earth magnetic field shielding for three different sized melt-textured YBCO samples as function of the flux gate sensor distance.

Therefore, to avoid the inevitable field trapping of B_{Earth} in the YBCO plate, a Helmholtz coil is used to compensate the applied field, at least in the center. Small deviations in the shielding behavior between the experimental and calculated curves for the three samples in Figure 3 indicate some imperfections in the B_{Earth}||a, b crystal orientation during field cooling. In evaluating the method, it should be noted that magnetic flux shielding with superconductors is an old concept. However, most approaches and models simulate active, driven magnetic coils [8]-[12]. In the closest position, about 2 mm above the YBCO plate, the earth field was reduced to less than 5 µT for a large 270 mm YBCO plate. Even for a smaller 130 mm plate, a shielding effect of about 9 µT/ 45 µT = 0.2 is observed.

Presumably, a significant portion of the residual flux still penetrates the polycrystalline melt processed YBCO, especially at the grain boundaries between the crystals. Increasing the distance to 200 mm above the back surface, the magnetic flux increases steeply and approaches 43 µT, which is close to the ambient value of the magnetic flux component measured by B_{Earth} for our Torgau site (48 µT).

3.2. Magnetic flux enhancement

For space applications, the Earth's magnetic field is the only readily available external working field. Therefore, all flux compression experiments were performed under B_{Earth} conditions, which are not constant due to the abrupt boundary between the magnetosphere and the surrounding plasma [14].

Additionally, the ISS is not in a geostationary orbit, it will rotate around the Earth's magnetic dipole. Magnetic data nearby superconductors for screening and compression will therefore need external reference measurements. The low Earth magnetic field shifts the experiments into the Meissner phase, consisting of surface currents and field-free regions (Figure 4, top). The magnitude of the compression is determined by the areas of the holes according to Equation 3. The final flux density is practically limited by a saturation value due to the critical current density J_c, the flux flow mechanism, and possible flux jump phenomena. The biggest handicap in achieving efficiency in mechanical compressor devices is caused by the small magnitude of the working field. The external earth magnetic field B_{Earth} of 30-50 µT used here shifts the compression mechanism from a bulk to a surface process

A surprising and promising experimental result of thermally induced flux enhancement is reported in Figure 4. During a transient warm-up process, an 8-crystal circular 110 mm YBCO plate shows an unexpectedly significant peak of about 125 µT, which is a factor of 2.5 higher than the ambient earth

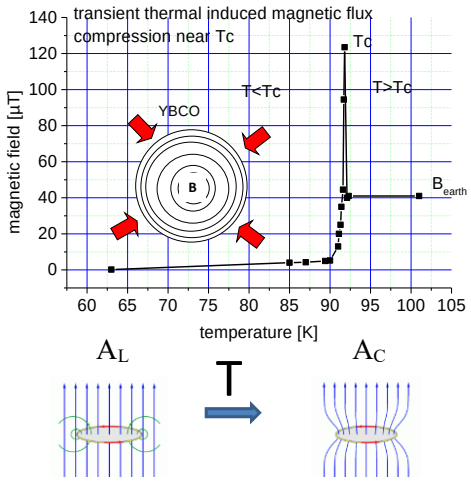

Figure 4. Thermally induced magnetic flux enhancement of a transient circular 110 mm YBCO plate.

field at the site. Using a tuned Helmholtz coil, the earth was completely compensated to zero for $T < T_c$. The YBCO plate was then cooled to below 65 K in a vacuum cryostat using a 3.5 W/80 K Stirling cryocooler (AIM, Germany). The Hall sensor was placed 2.5 mm above the YBCO plate and for $T < 80$ K the measured magnetic flux density behind the bulk was close to zero. Above 85 K, a small fraction (< 5 µT) of the field gradually penetrates the HTS, followed by a transient flux compression near $T_c = 92$ K with a short-lived peak above 120 µT. This experiment demonstrates the possibility of generating thermally induced earth magnetic peak flux densities significantly higher than the standard magnitude. This property was obtained in a transient heating process by reducing the flux active area according to formula (3).

With the above process, a similar experiment could be performed for the first time in space to increase the Earth's magnetic field for shielding purposes. According to the conservation of magnetic flux $\oint \boldsymbol{B} \times d\boldsymbol{S} = 0$ the total flux through a varying surface should be constant. The value of B_{peak} is obtained from Equation 3.

$$B_{peak} = B_{Earth} \frac{A_L}{A_C} \qquad (3),$$

where the areas of the load flux density and the compressed magnetic flux are A_L and A_C, respectively. B_{Earth} is the external working field, in our case the Earth's magnetic field with a strength of about 40 µT.

4. Proton irradiation of melt- textured YBCO bulk

ATZ Corp. has fabricated 8 PM rotor-YBCO stator systems with extremely low rotational friction for large-diameter cryogenic rotary stages to drive half-wave plate polarization modulation of cosmic microwave background (CMB) radiation detector systems. The size of the individual melt textured YBCO bulks was 40 mm x 40 mm at a thickness of 12 mm. The final diameter of the assembled YBCO rings fitted in a copper holder, varied between 120 mm and 556 mm. The fundamental advantage of a superconducting magnetic bearing over a mechanical bearing is the elimination of the stick-slip effect typical of mechanical ball bearings. The basis for all magnetic bearing applications is the magnetic force between a magnet and a superconductor, which is a function of the size of the flowing shielding current loop and the height of the critical current J_c. The force exerted by a magnet on a superconductor is given by the gradient of the volume integral,

$$\boldsymbol{F} = -\nabla \int \boldsymbol{M} \times \boldsymbol{B}\, dV \qquad (4),$$

where **M** is the magnetic moment of the superconductor and **B** is the magnetic flux density generated by the PM. The maximum levitation pressure is $P_{max} = B_r^2/2\mu_0$ when the critical current density is infinite (μ_0). For the currently available high-energy PMs (NdFeB, SmCo) with a surface induction $B_r \sim 1.0$ T, the pressure can reach about 4 bar. The maximum trapped field flux density in the z direction B_z^{max} of an infinitely long cylindrical sample with a diameter of 2R is then given by the relation

$$B_z^{max} = \mu_0 J_c^{\theta} R \qquad (5).$$

According to this equation, the maximum trapped field depends on the critical current density J_c and the diameter D = 2R of the superconducting domain. In practice, the value is reduced by geometrical and demagnetization effects. In the case of a radially symmetric geometry, $dB/dr = \mu_0 J_c$, integrated in the Bean model gives $B^* = \mu_0 J_c R$ for the maximum trapped magnetic flux B^*. Assuming a critical current of $J_c = 10^4$ A/cm² and a grain diameter of 2R = 40 mm, one approaches a trapped field value of $B^* = 1.2$ T.

Every SMB application in space is related to the question of whether Galactic Cosmic Rays (GCRs) outside the shielding Earth's magnetic field may contain particles dangerous to the superconductors. According to the analysis results of the Curiosity rover, the surface radiation environment of Mars has a galactic cosmic ray (GCR) influence that varies slightly depending on the solar modulation, with the proton abundance of 85 to 90%, helium ions ~10 to 13%, electrons ~1%, and ~1% heavier nuclei [13].

Less information is known about proton irradiation and the effect on the YBCO bulk superconductor. As the particle penetrates the medium, its energy loss per unit length changes. The energy loss of a particle is a function of its penetration distance. The energy loss increases toward the end of the range. Near the end, it reaches a maximum and then drops abruptly to zero. Proton irradiation experiments were conducted at the Heavy Ion Medical Accelerator (HIMAG) in Chiba, Japan.

Four single grain YBCO samples (2x 30 mm diameter, 2x 42 mm diameter) and two triple grain samples (64 x 32 x 12) were selected for investigation. All samples were measured using Hall scanning method with a constant activation field of 1.2 T and a waiting time of about 15 minutes. The YBCO samples were measured in their original state without any treatment and after irradiation with a typical medical dose of 10 kRAD for human application. 10 kRAD is equivalent to 100 GRAY (GY), which corresponds to an energy density of kg.

Table 1. Trapped magnetic flux measurements of melt-textured YBCO on proton irradiation

Sample YBCO	No Irrad.	10 kRAD	10+10 kRAD	No Irrad.
B_{max}[mT]	903	841	846	832/791
B_{av} [mT]	444	427	423	425/401

Compared to the as-grown flux density measurements, the proton beam tested YBCO samples show a relative change of the maximum magnetic flux ΔB_{max} = - 6.75% and on the integrated averaged flux ΔB_{av} = -3.75%, which is at the level of the untested YBCO samples variation of ΔB_{max} = -4.80% and ΔB_{av} = -3.55%. Hence, it is assumed that the performance of HTS bulk devices in space application due to proton impact shows no degradation in the critical current density and in the structure of the magnetic domains. According to Table I the samples with 10 kRAD + 10 kRAD proton irradiation show no changes in the trapped field measurements.

Additional pinning centers introduced in bulk superconductors depend on the size of the defects and the way they are created. The effect of neutron irradiation, which produces homogeneously distributed collision cascades similar to the size of the coherence length of the YBCO, is well known [15]. Since the neutron defects match the coherence length, the irradiation creates highly effective pinning centers.

Consequently, only a small surface depth of the YBCO samples would be affected by proton beam irradiation. Correspondingly, it was found that irradiation with moderate doses of high energy neutrons and charged particles results in a significant enhancement of magnetization and J_c due to the generation of additional flux pinning centers only in thin films.

5. Conclusion

Identical trapped flux measurements before and after the Blue Dot mission on the ISS and terrestrial irradiation experiments show HTS bulk material without significant changes. The melt-textured YBCO bulk interacts with the Earth's magnetic field, which has a magnitude of about 50 µT in central Europe, with the Meissner reaction type shielding the bulk from B_{Earth}. Near perfect B_{Earth} shielding as a function of sample size is demonstrated in laboratory experiments. A thermally induced reduction of the flux area shows a transient magnetic flux peak of 120 µT and corresponds to a compression increase of 250%.

6. References

[1] Werfel F N *et al* 2016 *IEEE Trans. Appl. Supercond.* vol. 25, 3 Impact of Cryogenics and Superconducting Components for HTS Magnetic Levitation Devices
[2] http://www.nasa.gov/mission_pages/station/research/experiments/1176. html, date 14.07. 2016
[3] Shu Q S *et al* 2006 *Cryogenics* vol 46, 2-3 pp 105-110
[4] Buckel W 1990 *Supraleitung* (VCH Verlagsgesellschaft mbH, Weinheim)
[5] Meissner W und Ochsenfeld R 1933 *Naturwissenschaften* vol 21 p 787
[6] Poole C *et al* 2010 *Superconductivity* (Academic Press)
[7] Pippard A 1950 *Proc. R. Soc. London, Ser. A* vol 203 p 210
[8] Hoffman J Fisher P and Batischev O 2005 *NIAC Phase I Final Report Contract CP 04-01* Use of Superconducting Magnet Technology for Astronaut Radiation Protection,
[9] Musenich R *et al* 2014 *IEEE Trans. Appl. Supercond.* A Magnesium Diboride Superconducting Toroid for Astroparticle Shielding vol 24 (3) p 4601504
[10] Battiston R *et al* 2013 *IEEE Trans. Appl. Supercond.* Superconducting magnets for astroparticle shielding in interplanetary manned missions vol 23 (3) p 4101604
[11] Ambroglini *et al* 2016 *Front. Oncol.* Evaluation of Superconducting Magnet Shield Configurations for Long Duration Manned Space Missions vol 6
[12] Hill C *et al* 2018 *arXiv: 1805.10403v1 [astro-ph.IM]*
[13] Hassler D *et al* 2014 *Science* Mars' Surface Radiation Environment Measured with the Mars Science Laboratory's Curiosity Rover vol 343
[14] Archer M *et al* 2019 *Nature Communications*, vol 10 p 615
[15] Sauerzopf F M 1998 PRB 57 10959